IEEE Access
Multidisciplinary | Rapid Review | Open Access Journal

Received March 16, 2021, accepted March 27, 2021, date of publication March 31, 2021, date of current version April 8, 2021.

Digital Object Identifier 10.1109/ACCESS.2021.3069994

Microwave Reflectometry to Characterize the Time-Varying Plasma Generated in the Shock Tube

LUTONG LI, (Student Member, IEEE), HAOQUAN HU, PU TANG, BO CHEN, JING TIAN, (Member, IEEE), AND BIXIAO JIANG

School of Electronic Science and Engineering, University of Electronic Science and Technology of China, Chengdu 611731, China

Corresponding author: Haoquan Hu (huhq@uestc.edu.cn)

ABSTRACT To investigate the behavior of plasma generated in the shock tube, microwave reflectometry is proposed to extract the permittivity ϵ_r of plasma. To remove the influence of parasitic reflections caused by the surroundings, a calibration process is introduced and the unknown calibration coefficients are determined by utilizing microwave interferometry as the reference technique. The shock tube is modeled as a three-layered medium to calculate the reflection coefficient. A time-dependent reconstruction algorithm is applied and theoretically validated to eliminate the multiple solutions in the inverse problem. By comparing the permittivities extracted with microwave reflectometry and interferometry, the effects of plasma diffusion are demonstrated with a modified analytical model in the beginning time region of experiments. In addition, the nonuniform flow in the generated plasma located near the end time region is also observed. The determination of the effective time region for electron density N_e and collision frequency v_e extraction is discussed as well. Finally, the differences between microwave reflectometry and interferometry in terms of averaged $N_e < 1\times10^{17}m^{-3}$ and averaged $v_e < 1.5\times10^{9}s^{-1}$ are investigated in the effective time region.

INDEX TERMS Microwave reflectometry, microwave interferometry, reflection coefficient, time-varying plasma, permittivity measurement, shock tube, electron density, collision frequency.

I. INTRODUCTION

During the atmosphere reentry of a spacecraft, the plasma or ionized gas layer surrounding the spacecraft forms a sheath [1]–[4] that intensively affects the radio frequency communication between spacecraft and ground station. Therefore, there has been significant interest in investigating the process of plasma formation and diagnostics of the plasma parameters. In [5], a semi-analytical self-consistent model was developed to studying the evolution of the plasma channel in conjunction with a fairly complete system of plasma chemical reactions. An fluid-dynamic model was introduced in [6] to describe a focused microwave discharge in a molecular gas and investigate the main spatial–temporal parameters of the plasma formed at the main focus of the system. Shock tubes, in which the supersonic gas flows are generated, are also widely used to study the plasmas and related phenomena [7]–[9]. To characterize the properties of plasma inside the shock tube, microwave interferometry [10], [11] based on the amplitude attenuation and phase shift induced by plasma were applied. However, as the amplitude attenuation increases, the strength of transmitted signals drops below the noise floor of microwave receiver, resulting in the failure of microwave interferometry. On the contrary, microwave reflectometry exhibits the potential in the characterization of high-density plasma due to the increased amplitude of the reflected signals compared with the low-density case [12].

Microwave reflectometry is often employed for the purpose of diagnosis and monitoring [13]. For the application of plasma diagnostics, most microwave reflectometries are related to the radar techniques in the time-domain and dedicated to the fusion plasma with various techniques such as amplitude modulation (AM) reflectometry [14]–[17], frequency modulation (FM) reflectometry [18], [19], and pulsed reflectometry [20]–[22]. However, the plasma generated in the shock tube is about a few hundred microseconds, making it hard to implement the modulation techniques. The parasitic reflections [22] caused by surroundings also act as an essential role in the diagnosis and interfere with the desired reflection of generated plasma. The system

The associate editor coordinating the review of this manuscript and approving it for publication was Abhishek K. Jha.

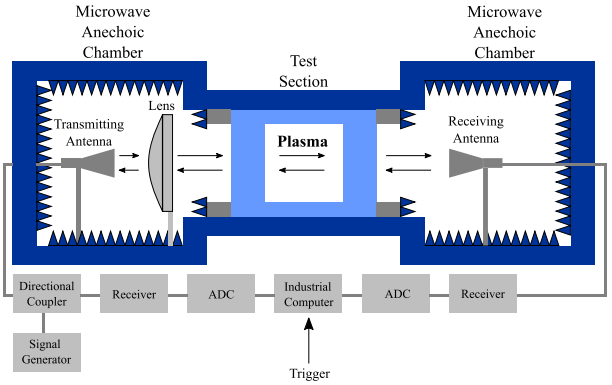

FIGURE 1. The experiment schematic of microwave reflectometry associated with microwave interferometry.

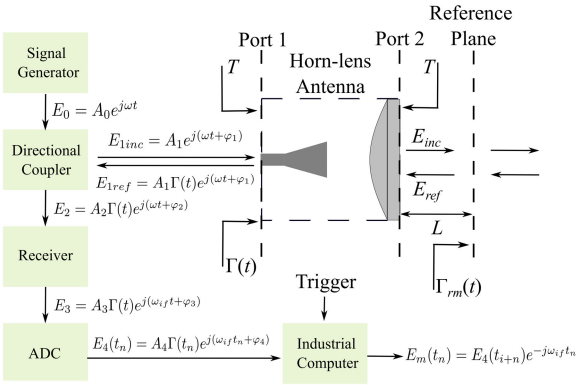

FIGURE 2. The signal flowchart of microwave reflectometry.

reflection in the monostatic setup also leads to a significant deviation that certainly affects the characterization results. The theoretical treatment of microwave propagating inside the plasmas is also a significant aspect for microwave diagnostics, and extensively studied in past decades [23], [24]. However, the numerical analysis of microwave incident on a plasma slab exhibits large fluctuations [9], [25]–[28] in the reflection properties, resulting in multiple solutions in the inverse problem, which also need to be properly addressed.

In this article, microwave reflectometry operating at a single frequency is proposed to extract the permittivity of plasma generated in the shock tube. To extract the reflection coefficient from the measured reflected signal, a signal model of microwave reflectometry and the corresponding calibration technique are introduced to reduce the influence of the parasitic reflections. The analytical model of plane wave incident on the shock tube is established based on the three-layered medium structure to calculate the reflection coefficient. A time-dependent reconstruction algorithm is applied to extract ϵ_r from the reflection coefficient. To determine the unknown calibration coefficient, microwave interferometry is employed as a reference technique. The measurement setup with both microwave reflectometry and interferometry are shown in Fig. 1, in which both systems are activated simultaneously to measure the permittivity of plasma. The extracted ϵ_r of microwave reflectometry and interferometry are compared with each other to investigate the behavior of plasma. As all extracted ϵ_{ri} by microwave interferometry meet the condition of $\epsilon'_{ri} < 1$ and $\epsilon''_{ri} < 0$, microwave reflectometry exhibits the limited effective time region of the analytical model. In the effective time region, the extracted N_e and ν_e of microwave reflectometry and interferometry are investigated as well. In Sec. II, the detailed description of theory and setup of microwave reflectometry are presented. The numerical analysis of the inverse problem in microwave reflectometry is conducted in Sec. III. The combined experiments of microwave reflectometry and interferometry are analyzed and discussed in Sec. IV. Conclusions are given in Sec. V.

II. THE DETAILED DESCRIPTION OF MICROWAVE REFLECTOMETRY

A. CALIBRATION OF THE MEASURED REFLECTION COEFFICIENT AT THE REFERENCE PLANE TO REMOVE THE INFLUENCE OF PARASITIC REFLECTIONS

As shown in Fig. 1, the proposed microwave reflectometry consists of a signal generator, directional coupler, receiver, analog to digital converter (ADC), and horn-lens antenna. Microwave anechoic chambers are employed to reduce the undesired scatterings caused by the background. The measured transmitted and reflected signals are both recorded by an industrial computer. To illustrate the measurement process, a signal model of microwave reflectometry is presented in Fig. 2. The signal generator is connected to the directional coupler, which is then connected to the horn-lens antenna. The horn-lens antenna operates as a reciprocal waveguide to free-space transmission line convertor [29], resulting in identical transmission coefficients (i.e., T) on port 1 and 2. The distance between port 2 and the reference plane is L. $\Gamma_{rm}(t)$ is the measured reflection coefficient at the reference plane, and the reflection coefficient at port 1 can be written as [29]

$$\Gamma(t) = |\Gamma(t)|e^{j\varphi_r(t)} = \Gamma_0 + T\Gamma_{rm}(t)Te^{-2jk_0L}, \qquad (1)$$

where k_0 is the wavenumber in free-space. The time-independent reflection coefficient $\Gamma_0 = |\Gamma_0|e^{j\varphi_{r0}}$ is determined by the self-reflection and parasitic reflections caused by the surroundings. The directional coupler also functions to transmit the reflected signal to the receiver, which converts the signal frequency ω down to the intermediate frequency ω_{if}. ADC converts the analog signals to the digital signals with the sampling time interval Δt, thus t is discretized as $t_n = n\Delta t$. A_i/A_1 and $\varphi_i - \varphi_1$(i.e., $i = 2, 3, 4$) represent the amplitude attenuation and phase shift of each output port caused by system components respectively. As the trigger signal is generated by an external device, a time delay $t_i = i\Delta t$ is introduced in the baseband signal of industrial computer $E_m(t_n) = A_m(t_n)e^{j\varphi_m(t_n)}$ to indicate the random experiment

recording time as

$$E_m(t_n) = A_4|\Gamma(t_{i+n})|e^{j[\varphi_r(t_{i+n})+\omega_{if}t_i+\varphi_4]}. \quad (2)$$

Based on the signal model, the corresponding calibration is introduced as follows. At the initial moment t_0, the shock tube is full of air, and the reflection coefficient at the reference plane is Γ_{rair}. The reflection coefficient at port 1 is written as

$$\Gamma(t_0) = \Gamma_0 + T\Gamma_{rair}Te^{-2jk_0L}. \quad (3)$$

Refer to (1) and (3), $\Gamma_{rm}(t)$ can be derived as

$$\Gamma_{rm}(t) = \frac{\Gamma(t)-\Gamma_0}{\Gamma(t_0)-\Gamma_0}\Gamma_{air}. \quad (4)$$

Substituting $\Gamma(t)$ with $E_m(t_n)$, (4) is rewritten as

$$\Gamma_{rm}(t_n, A_s, \varphi_s) = \frac{E_m(t_n)-S}{E_m(t_0)-S}\Gamma_{air}, \quad (5)$$

where $S = A_s e^{j\varphi_s} = A_4|\Gamma_0|e^{j(\varphi_{r0}+\omega_{if}t_i+\varphi_4)}$ is the unknown calibration coefficient which is time-independent during the experiment. Under the same experiment setup, the parasitic reflections remain unchanged, and thus A_s is a constant. Due to the random trigger time, t_i is not a constant in different experiments, resulting in the difficulty to extract $\Gamma_{rm}(t_n)$ directly. It should be noted that both $\varphi_m(t_0) = \varphi_r(t_0)+\omega_{if}t_i+\varphi_4$ and $\varphi_s = \varphi_{r0}+\omega_{if}t_i+\varphi_4$ contain $\omega_{if}t_i$, resulting in the same phase differece (i.e., $\Delta\varphi = \varphi_m(t_0)-\varphi_s$) in each experiment. Therefore, based on the invariable A_s and $\Delta\varphi$, a calibration experiment with known S is required, and S' of another experiment can be determined as

$$A_s' = A_s, \quad (6)$$

and

$$\varphi_s' = \varphi_m'(t_0) + \varphi_s - \varphi_m(t_0). \quad (7)$$

B. THE ANALYTICAL MODEL OF THE SHOCK TUBE TO CALCULATE THE REFLECTION COEFFICIENT AT THE REFERENCE PLANE

The permittivity ϵ_r of plasma is assumed to be of Drude type [26] as

$$\epsilon_r = \epsilon_r' + j\epsilon_r'' = 1 - \frac{\omega_{pe}^2}{4\pi^2(f^2+\nu_e^2)} - j\frac{\nu_e}{f}\frac{\omega_{pe}^2}{4\pi^2(f^2+\nu_e^2)}, \quad (8)$$

where f is operation frequency, and ν_e is collision frequency. ω_{pe} is related to electron density N_e and defined as

$$\omega_{pe} = \sqrt{\frac{N_e e^2}{\epsilon_0 m_e}}, \quad (9)$$

where ϵ_0 is the permittivity of vacuum. e and m_e are respectively the electron charge and mass.

To derive the formulas of the reflection coefficient Γ_r at the reference plane with ϵ_r, the generated plasma filled the tube is assumed uniform so that the shock tube can be modeled as a three-layered medium structure as illustrated in Fig. 3. The wall of the shock tube is made of Polytetrafluoroethylene (PTFE), which permittivity is ϵ_{rt}, and the thickness d_1 is

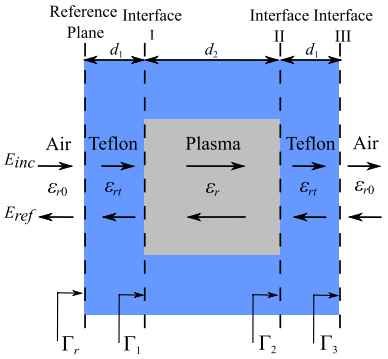

FIGURE 3. The analytical model of the shock tube.

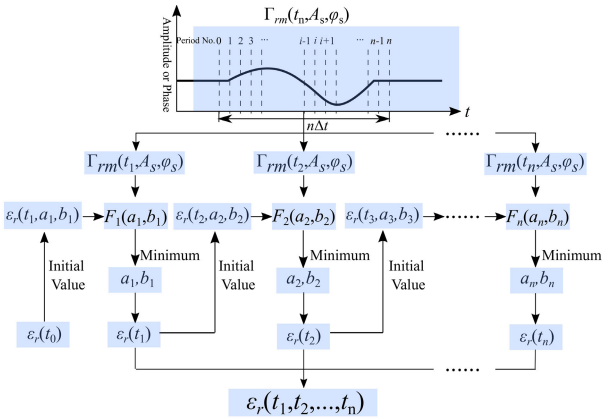

FIGURE 4. The flowchart of time-dependent reconstruction algorithm in the extraction of $\epsilon_r(t_n)$ from $\Gamma_{rm}(t_n, A_s, \varphi_s)$.

3.5 cm. The inner width d_2 of the shock tube is 8 cm. The incident wave is assumed as the uniform plane wave and the boundary matching conditions of electric and magnetic fields at each interface are applied to calculate the reflection coefficient. The reflection coefficient Γ_3 at Interface III is derived as

$$\Gamma_3 = \frac{\eta_0-\eta_1}{\eta_0+\eta_1}e^{-2jk_1(2d_1+d_2)}, \quad (10)$$

where η_0 and $\eta_1 = \eta_0/\sqrt{\epsilon_{rt}}$ are the characteristic impedance of air and PTFE. k_0 and $k_1 = k_0\sqrt{\epsilon_{rt}}$ are the wavenumber in air and PTFE. The reflection coefficient Γ_2 at Interface II is written as

$$\Gamma_2 = \frac{(\eta_1-\eta)+(\eta_1+\eta)\Gamma_3 e^{2jk_1(d_1+d_2)}}{(\eta_1+\eta)+(\eta_1-\eta)\Gamma_3 e^{2jk_1(d_1+d_2)}}e^{-2jk(d_1+d_2)}, \quad (11)$$

where $\eta = \eta_0/\sqrt{\epsilon_r}$ is the characteristic impedance of plasma and $k = k_0\sqrt{\epsilon_r}$ is the wavenumber in plasma. The reflection coefficient Γ_1 at Interface I is derived as

$$\Gamma_1 = \frac{(\eta-\eta_1)+(\eta+\eta_1)\Gamma_2 e^{2jkd_1}}{(\eta+\eta_1)+(\eta-\eta_1)\Gamma_2 e^{2jkd_1}}e^{-2jk_1d_1}, \quad (12)$$

and Γ_r is derived as

$$\Gamma_r = \frac{(\eta_1-\eta_0)+(\eta_1+\eta_0)\Gamma_1}{(\eta_1+\eta_0)+(\eta_1-\eta_0)\Gamma_1}. \quad (13)$$

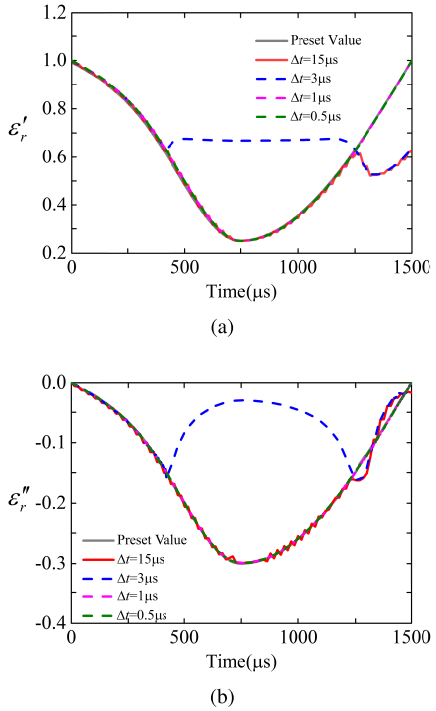

FIGURE 5. The numerical analysis of the inverse problem with the calculated $\Gamma_r(t_n)$ under different Δt (15 μs, 3 μs, 1 μs, and 0.5 μs). (a) the retrieved $\epsilon_r'(t_n)$, and (b) the retrieved $\epsilon_r''(t_n)$.

C. THE TIME-DEPENDENT RECONSTRUCTION ALGORITHM FOR THE EXTRACTION OF PERMITTIVITY

As the dimensions and dielectric properties of shock tube are already known, Γ_r is expressed as a function of ϵ_r, and ϵ_r can be determined by matching the measured reflection coefficient Γ_{rm} with $\Gamma_r(\epsilon_r)$. Due to the existence of multiple solutions, it is necessary to utilize the predefined bounding constraints to extract ϵ_r from Γ_{rm} [9]. However, in the shock tube experiment, it is hard to estimate the ϵ_r constraints of generated plasma. Therefore, a linear variation approximation was proposed in our preliminary work [30] to solve the inverse problem. By applying the approximation to ϵ_r during the sampling time interval Δt between two adjacent sampling points of the high-speed ADC, a time-dependent reconstruction algorithm is introduced and the detailed description is presented in Fig. 4. Γ_{rm} is discretized as a n-points sequence in time domain with Δt, and $\epsilon_r(t_i)$ is written as

$$\epsilon_r(t_i, a_i, b_i) = [\epsilon_r'(t_{i-1}) + a_i\Delta t] + j[\epsilon_r''(t_{i-1}) + b_i\Delta t], \quad (14)$$

where $\epsilon_r'(t_{i-1})$ and $\epsilon_r''(t_{i-1})$ are the values of the previous sampling point while a_i and b_i are unknown gradients of ϵ_r' and ϵ_r'', respectively. The objective function is defined as

$$F_i(a_i, b_i) = |\Gamma_{rm}(t_i, A_s, \varphi_s) - \Gamma_r(\epsilon_r(t_i, a_i, b_i))|. \quad (15)$$

By minimizing $F_i(a_i, b_i)$, a_i and b_i can be determined to retrieve $\epsilon_r(t_i)$. Before the plasma is generated, the initial value $\epsilon_r(t_0) = 1$, which equals to the permittivity of air, is applied to extract a_1 and b_1. Once $\epsilon_r(t_1)$ is retrieved, $\epsilon_r(t_1)$ become the initial value of $\epsilon_r(t_2)$ and is applied to determine a_2 and b_2. The rest of sequence $\epsilon_r(t_n)$ can be achieved in the same manner. v_e and N_e can also be extracted from ϵ_r respectively as

$$v_e = \frac{\epsilon_r'' f}{\epsilon_r' - 1}, \quad (16)$$

and

$$N_e = \frac{m_e\epsilon_0(1-\epsilon_r')4\pi^2(f^2+v_e^2)}{e^2}. \quad (17)$$

III. THE NUMERICAL ANALYSIS OF THE INVERSE PROBLEM

Referring to [9], it is found that the same Γ_r can be achieved with different values of ϵ_r in (13), resulting in multiple minima in the extraction of ϵ_r. To verify the effectiveness of time-dependent ϵ_r reconstruction algorithm to eliminate the effects of multiple solutions, the numerical analysis based on the calculated $\Gamma_r(t)$ from the preset $\epsilon_r(t)$ is conducted. Two functions, as illustrated in (18) and (19), are utilized to describe $\epsilon_r(t) = \epsilon_r'(t) + j\epsilon_r''(t)$ of time-varying plasma.

$$\epsilon_r'(t) = \begin{cases} 1 - \alpha[\sin(\frac{\pi t}{n\Delta t}) \\ +\sin^3(\frac{\pi t}{n\Delta t}) + \sin^5(\frac{\pi t}{n\Delta t})], & t \in (0, \frac{n\Delta t}{2}) \\ 1 - 3\alpha\sin(\frac{\pi t}{n\Delta t}), & t \in (\frac{n\Delta t}{2}, n\Delta t) \end{cases} \quad (18)$$

$$\epsilon_r''(t) = \begin{cases} -\beta[\sin(\frac{\pi t}{n\Delta t}) \\ +\sin^3(\frac{\pi t}{n\Delta t}) + \sin^5(\frac{\pi t}{n\Delta t})], & t \in (0, \frac{n\Delta t}{2}) \\ -3\beta\sin(\frac{\pi t}{n\Delta t}), & t \in (\frac{n\Delta t}{2}, n\Delta t) \end{cases} \quad (19)$$

where the coefficients $\alpha = 0.25$ and $\beta = 0.1$ are used in the numerical case. The total time (i.e., $n\Delta t$) of 1500 μs is used in the analysis. The operating frequency f is 10 GHz. The analytical model presented in Fig. 3 is used and the accuracy of the time-dependent ϵ_r reconstruction algorithm is determined by the linearity of $\epsilon_r(t_n)$ between two sampling time points, which can be improved with the decrease of Δt. To investigate the effect of Δt, various Δt (i.e., 15 μs, 3 μs, 1 μs, and 0.5 μs) are applied in the calculation of $\Gamma_r(t_n)$. The preset and retrieved $\epsilon_r(t_n)$ are presented in Fig. 5. The fluctuations observed in the retrieved $\epsilon_r'(t_n)$ and $\epsilon_r''(t_n)$ utilizing $\Delta t = 15$ μs reveal the fact that $\epsilon_r(t_n)$ is undersampled. As Δt decreases to 3 μs, the effects of multiply solutions appear, leading to the large deviations between preset and retrieved curves. For the case of 1 μs and 0.5 μs, the retrieved plots of $\epsilon_r(t_n)$ match well with that of $\epsilon_r(t)$, which validates the proposed time-dependent ϵ_r reconstruction algorithm and demonstrates the decrease of Δt is an effective approach to eliminate the multiply solutions and improve the accuracy of retrieved results.

IV. EXPERIMENT AND DISCUSSION

A. THE EXPERIMENT SETUP

As shown in Fig. 6, the shock tube employed to generate plasma consists of a driver section, a driven section, and a test

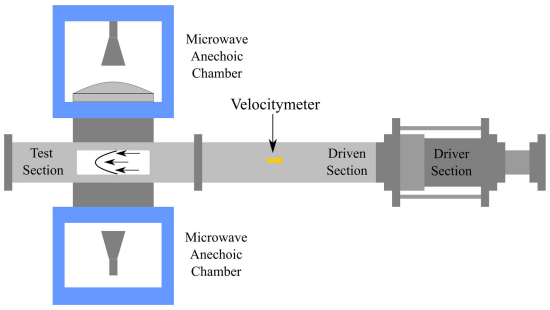

FIGURE 6. Schematic of the shock tube and the experiment setup.

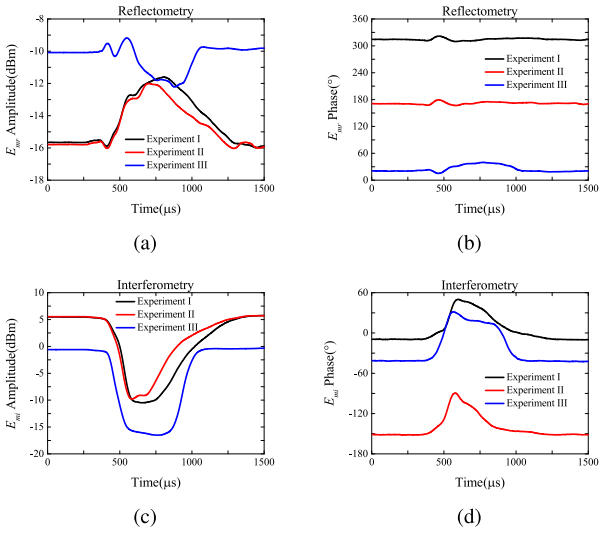

FIGURE 7. The measured base-band signal E_{mr} and E_{mi}.

section. The driver section is filled with a mixture of driving gases containing O_2, H_2, and N_2 at high pressure. The driven section is vacuumed to low pressure. The test section is the extension of the driver section for experimental investigations of the excited plasma. An aluminum diaphragm connecting with a condenser bank is inserted to separate the driver section from the driven section. To generate the shock wave, the condenser bank is charged to a voltage of 3.4 kV to ignite the mixed gas. As a result of the discharge, it ruptures the aluminum diaphragm and generates a shock wave in the driven section. The velocity meter is installed in the driven section to measure the speed v_f of shock wave and generate the trigger signal. Microwave interferometry and reflectometry are both placed at the test section to characterize the ϵ_r of plasma. The operation frequency is $f = 5.8$ GHz. $\Delta t = 0.5$ μs, which has been proved as a good sampling time interval for the extraction of ϵ_r, is used in the following analysis.

B. THE VALIDATION OF THE CALIBRATION PROCESS IN MICROWAVE REFLECTOMETRY

In this section, three experiments are conducted to verify the calibration process of $\Gamma_{rm}(t_n, A_s, \varphi_s)$. The experiment setup

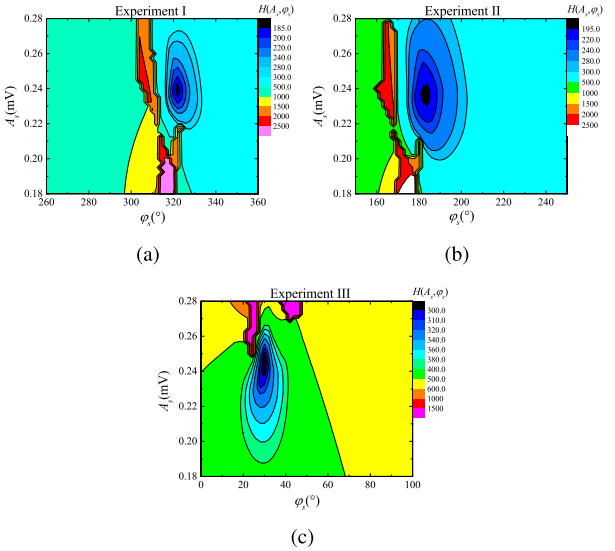

FIGURE 8. Surface plots of the calculated $H(A_s, \varphi_s)$. (a) experiment I, (b) experiment II, and (c) experiment III.

of all experiments remains the same except that in the last experiment the output power of microwave signal generator is lowered to illustrate the validation of proposed calibration process under varying output signal strength.

The measured baseband signals E_{mr} and E_{mi} of microwave reflectometry and interferometry, respectively, are presented in Fig. 7. It is noted that both the amplitude and phase plots of E_{mi} are similar to each other for all experiments. However, the plot of E_{mr} for experiment III exhibits significant differences in both amplitudes and phases compared with the other two cases. The permittivity of microwave interferometry (i.e., $\epsilon_{ri}(t)$) is directly extracted from the phase shift $\Delta\varphi_i = \varphi_i(t) - \varphi_i(t_0)$ and attenuation $\Delta A_i = A_i(t)/A_i(t_0)$ of $E_{mi} = A_i(t)e^{j\varphi_i(t)}$ as [10], [11]

$$\epsilon_{ri}(t) = [-\frac{\Delta\varphi_i}{k_0 d_2} + 1 + j(\frac{\ln \Delta A_i}{k_0 d_2})]^2. \tag{20}$$

For microwave reflectometry, the initial value of A_s and φ_s are to be determined before the extraction of $\epsilon_r(t)$. Based on the assumed condition of $\epsilon_{ri}(t) = \epsilon_r(t, A_s, \varphi_s)$, A_s and φ_s can be determined by minimizing the following objective function

$$H(A_s, \varphi_s) = \sum_{i=1}^{n} |\epsilon_r(t_i, A_s, \varphi_s) - \epsilon_{ri}(t_i)|. \tag{21}$$

The calculated $H(A_s, \varphi_s)$ of experiment I-III are illustrated in Fig. 8. The extracted A_s and φ_s are presented in Table 1. It is noted all extracted A_s are around 0.24 mV, and the extracted phase differences $\Delta\varphi$ are also in good agreement with each other, demonstrating the validity of the calibration process.

To make a comparison between $\epsilon_r(t)$ and $\epsilon_{ri}(t)$, $A_s = 0.24$ mV and $\Delta\varphi = 7°$ achieved from experiment I are used to extract $\epsilon_r(t)$ for all experiments. Thus, A_s in experiment II and III are also set as 0.24 mV, and φ_s in experiment II and III are respectively set as 178° and 28°

TABLE 1. The extracted A_s and $\Delta\varphi$ in the experiments.

Experiment	A_s(mV)	$\varphi_s(^\circ)$	$\varphi_m(t_0)(^\circ)$	$\Delta\varphi(^\circ)$
I	0.240	322	315	7
II	0.238	182	171	11
III	0.245	30	21	9

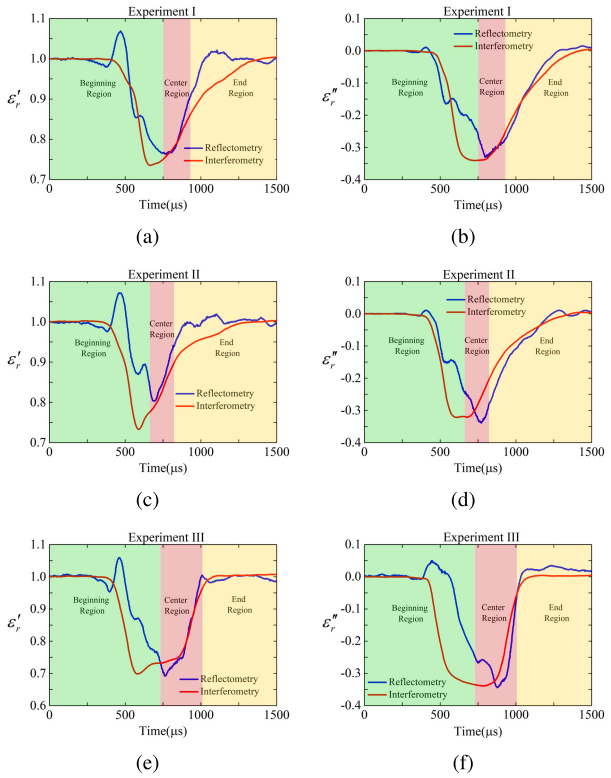

FIGURE 9. The comparison of extracted ϵ_r by microwave reflectometry and extracted ϵ_{ri} by microwave interferometry in experiment I-III. The matched regions of ϵ_r and ϵ_{ri} are marked as the center region, and the other regions are marked as the beginning and end regions.

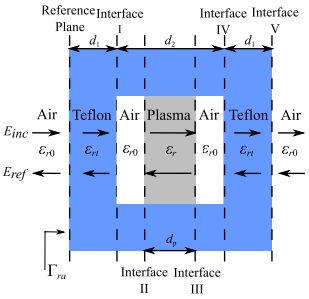

FIGURE 10. The modified analytical model of the shock tube with two inserted airgap layers.

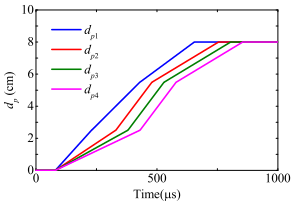

FIGURE 11. The assumed curves of d_p.

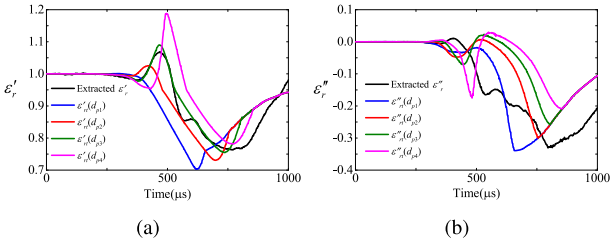

FIGURE 12. The comparison of extracted ϵ_r by microwave reflectometry and retrieved ϵ_{rt} from Γ_{ra} with the assumed d_p (i.e., d_{p1}, d_{p2}, d_{p3}, and d_{p4}) in experiment I. Γ_{ra} is calculated from extracted ϵ_{ri} by microwave interferometry referring to the modified analytical model.

referring to (6) and (7). The extracted $\epsilon_r(t)$ and $\epsilon_{ri}(t)$ of experiment I-III are presented in Fig. 9. It is observed that the extracted $\epsilon_r(t)$ and $\epsilon_{ri}(t)$ agree well only in the limited time region, which is marked as the center region. The other regions are marked as the beginning and end regions, in which the large deviations between $\epsilon_r(t)$ and $\epsilon_{ri}(t)$ are observed. The possible reasons resulting in the deviations are discussed in the following subsection.

C. THE ANALYSIS OF EXTRACTED PERMITTIVITY OF MICROWAVE REFLECTOMETRY IN THE BEGINNING AND END REGIONS

In the beginning regions, both the real and imaginary parts of extracted $\epsilon_r(t)$ show an unexpected peak with $\epsilon_r' > 1$ and $\epsilon_r'' > 0$. This is possible because the generated plasma is in the diffusion process and not full of the shock tube. To investigate this phenomenon, a numerical analysis is conducted based on a modified analytical model of the shock tube, in which two airgap layers are added between plasma and the wall of shock tube on both sides, as shown in Fig. 10. Hence, the shock tube is modeled as a 5-layered medium and the reflection coefficient Γ_{ra} at the reference plane can be calculated in the same manner with Γ_r. d_p is the width of plasma and assumed as a time-dependent function. To analyze the effects of the airgap layers, the extracted $\epsilon_{ri}(t)$ by microwave interferometry in experiment I is used as the preset value to calculate the reflection coefficient $\Gamma_{ra}(t)$ based on the modified model. By utilizing the analytical model in Fig. 3, the retrieved permittivity $\epsilon_{rt}(t)$ from $\Gamma_{ra}(t)$ is compared with the extracted $\epsilon_r(t)$ by microwave reflectometry in experiment I.

As shown in Fig. 11, the width of plasma is assumed as functions of time (i.e., d_{p1}, d_{p2}, d_{p3}, and d_{p4}), and the corresponding retrieved $\epsilon_{rt}(t)$ are presented in Fig. 12. It can be seen that when d_p is increased from 0 cm to 8 cm, the phenomenon of $\epsilon_r' > 1$ and $\epsilon_r'' > 0$ is well reproduced in Fig. 12, indicating the effectiveness of the proposed assumption. In addition, the retrieved $\epsilon_{rt}'(t)$ of d_{p3} agree well with the extracted $\epsilon_r'(t)$, and the variation trend of $\epsilon_{rt}''(t)$ in time domain is also similar with the extracted $\epsilon_r''(t)$. However,

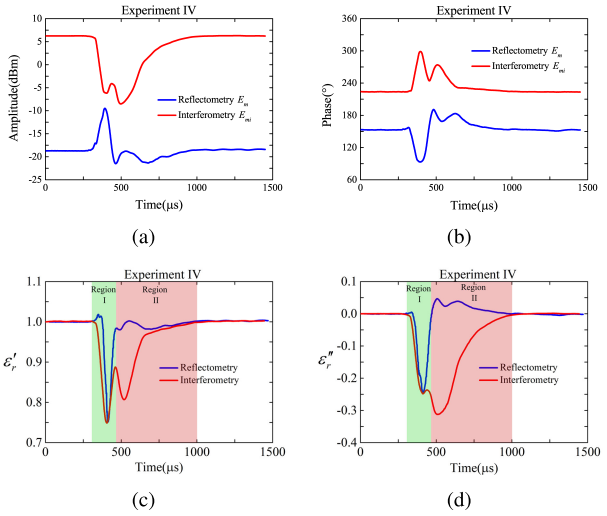

FIGURE 13. (a) and (b) are the measured amplitudes and phases of E_{mr} and E_{mi} in experiment IV. (c) and (d) are the comparison of extracted ϵ_r by microwave reflectometry and extracted ϵ_{ri} by microwave interferometry, which are divided into two regions (i.e., region I and region II) in time domain.

TABLE 2. Experiment parameters inside the shock tube.

Experiment	Gases Ratio(O_2, H_2, N_2)	v_f(km/s)
I-III	2.4:10.6:5	2.8
IV	1.6:11.4:5	4.2

large deviations between $\epsilon_{rt}''(t)$ and $\epsilon_r''(t)$ are still observed. The possible reason is that the effects of the radiation beam divergence are not considered, which can certainly result in the oblique incident waves near the edges of the shock tube. As shown in Fig. 1, for microwave interferometry only the transmitted waves around the central region of the shock tube, in which the effects of the oblique waves are reduced, can be received. On the contrary, for microwave reflectometry the horn-lens antenna exhibiting a larger radiation aperture can still receive the oblique reflected waves. Due to the polarization, incident angle, and propagation path deflections induced by plasma [27], the undesired oblique reflected waves are partly received, leading to more propagation loss than the normal incident case.

During the end regions, experiment I and II exhibit larger deviations between $\epsilon_r'(t)$ and $\epsilon_{ri}'(t)$ in comparison with the well-matched $\epsilon_r''(t)$ and $\epsilon_{ri}''(t)$. Besides, the small fluctuations are also observed in the extracted $\epsilon_r(t)$ of experiment III. These phenomenons can be attributed to the nonuniform flow. To illustrate the effects of the nonuniform flow, a typical experiment (i.e., experiment IV) with a higher v_f is also conducted, and the experiment parameters are illustrated in Table 2. $A_s = 0.33$ mV and $\varphi_s = 118°$ are used in the calibration. The measured E_{mr} and E_{mi} are presented in Fig. 13(a) and 13(b). The extracted ϵ_r and ϵ_{ri} are shown in Fig. 13(c) and 13(d). It is noted that the comparison of ϵ_r and ϵ_{ri} reveals that the observed plasma is divided into two regions (i.e., region

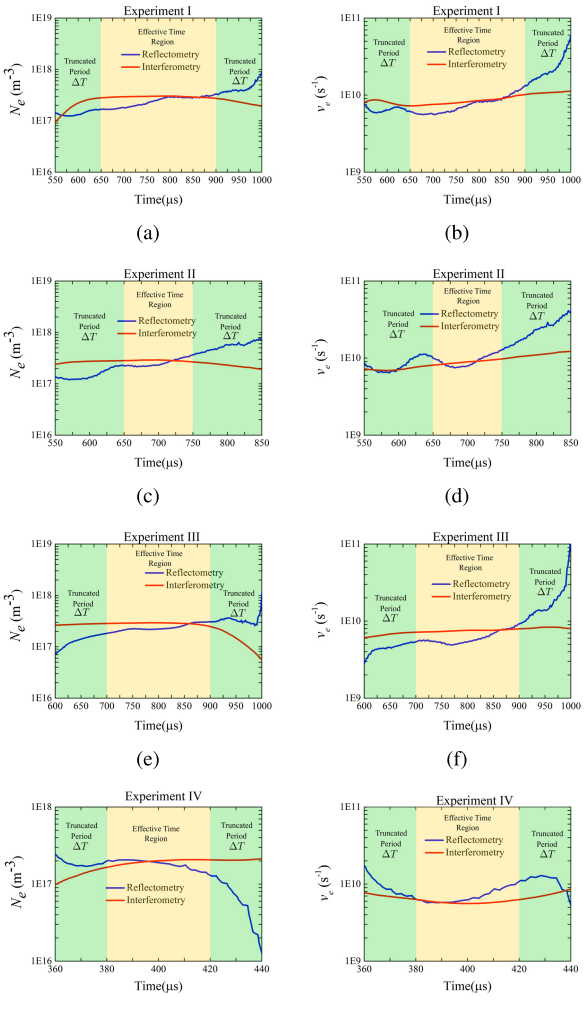

FIGURE 14. The extracted N_e and v_e by microwave reflectometry and interferometry in the limited time region with the constrains: $\epsilon_r' < 1$ and $\epsilon_r'' < 0$. The truncated period ΔT is introduced in the calculation of average value to remove the effects of plasma diffusion and nonuniform flow.

I and region II), consistent with the analysis presented in [7]. Due to the differences in their formation mechanisms, these two regions exhibit distinctive transmission and reflection responses. It can be seen that in region I both ϵ_r' and ϵ_r'' extracted from microwave reflectometry and interferometry agree well with each other, demonstrating the effectiveness of the assumption of uniform plasma distribution. However, due to the presence of the nonuniform flow, the ϵ_r' and ϵ_r'' extracted from microwave reflectometry and interferometry exhibit a significant difference in region II, revealing that region II should not be considered in the calculation of N_e and v_e due to the inaccurate description of the analytical model.

D. THE COMPARISON OF EXTRACTED ELECTRON DENSITY AND COLLISION FREQUENCY BETWEEN MICROWAVE REFLECTOMETRY AND INTERFEROMETRY

In the diagnosis of shock tube excited plasma utilizing microwave reflectometry or interferometry, it is assumed that

TABLE 3. The average value of extracted N_e and v_e.

Experiment	Reflectometry		Interferometry	
	$N_e(m^{-3})$	$v_e(s^{-1})$	$N_e(m^{-3})$	$v_e(s^{-1})$
I	2.42×10^{17}	7.65×10^{9}	2.92×10^{17}	8.31×10^{9}
II	2.59×10^{17}	9.26×10^{9}	2.83×10^{17}	8.89×10^{9}
III	2.37×10^{17}	6.12×10^{9}	2.84×10^{17}	7.50×10^{9}
IV	1.82×10^{17}	7.12×10^{9}	1.87×10^{17}	6.00×10^{9}

the whole shock tube is filled with the uniform plasma. However, this assumption is not valid in the beginning and end time regions of the experiment. Therefore, the analytical model is only effective in extracting N_e and v_e within a limited time region. For the presented experiments, the effective time regions are initially determined as 550 μs to 1000 μs, 550 μs to 850 μs, 600 μs to 1000 μs, and 360 μs to 440 μs with the constrains: $\epsilon_r' < 1$ and $\epsilon_r'' < 0$, as shown in Fig. 14. It can be seen that these time regions not only cover the matched regions of ϵ_r and ϵ_{ri} but also the regions with considerable differences. Besides, the extracted N_e and v_e also exhibit noticeable differences near the beginning and ending regions, which are induced by the effects of plasma diffusion and nonuniform flow in shock tube, respectively. Therefore, the effective time region is finally determined by truncating $N_e(t)$ and $v_e(t)$ with a time period ΔT at the beginning and end parts to remove the effects. In experiment I-III, $\Delta T = 100$ μs is used. In experiment IV, as v_f is increased from 2.8 km/s to 4.2 km/s, the duration of the limited time region is compressed and the effective time region is confirmed as 380 μs to 420 μs with $\Delta T = 20$ μs. The extracted $N_e(t)$ and $v_e(t)$ by microwave reflectometry and interferometry in the effective time regions are averaged as the typical values to be compared. As presented in Table 3, the differences of averaged N_e are less than $1\times10^{17}m^{-3}$, and the differences of averaged v_e are less than $1.5\times10^{9}s^{-1}$, demonstrating the accuracy of microwave reflectometry.

V. CONCLUSION

This article presents microwave reflectometry for plasma diagnosis, including the calibration of the base-band signals, the analytical model derivation of the shock tube, and the time-dependent algorithm to solve the inverse problem. Both microwave reflectometry and interferometry are applied to characterize the time-varying plasma generated in the shock tube. The calibration is testified with three experiments conducted under identical conditions. The extracted ϵ_r and ϵ_{ri} show good agreement in the center time region. The phenomenon of $\epsilon_r' > 1$ and $\epsilon_r'' > 0$ is observed in the beginning time region, which is analyzed with a modified analytical model to demonstrate the effects of plasma diffusion. An additional high v_f experiment is also conducted to illustrate the difference between uniform and nonuniform flows. The effective time region is determined by excluding the time regions with plasma diffusion and nonuniform flows to extract $N_e(t)$ and $v_e(t)$. The averaged N_e and v_e measured with microwave reflectometry and interferometry are also compared with each other, demonstrating the differences less than $1\times10^{17}m^{-3}$ and $1.5\times10^{9}s^{-1}$ respectively.

REFERENCES

[1] J. Rybak and R. J. Churchill, "Progress in reentry communications," *IEEE Trans. Aerosp. Electron. Syst.*, vol. AES-7, no. 5, pp. 879–894, Sep. 1971.
[2] M. Jung, H. Kihara, K.-I. Abe, and Y. Takahashi, "Reentry blackout prediction for atmospheric reentry demonstrator mission considering uncertainty in chemical reaction rate model," *Phys. Plasmas*, vol. 25, no. 1, Jan. 2018, Art. no. 013507.
[3] A. Mousavi, A. Esfandiari-Kalejahi, and M. Akbari-Moghanjoughi, "Nonextensivity effect on radio-wave transmission in plasma sheath," *Phys. Plasmas*, vol. 23, no. 4, Apr. 2016, Art. no. 043516.
[4] Q. Zhao, Y. Bo, M. Lei, S. Liu, Y. Liu, J. Liu, and Y. Zhao, "Numerical evaluation of external magnetic effect on electromagnetic wave transmission through reentry plasma layer," *Phys. Plasmas*, vol. 23, no. 11, Nov. 2016, Art. no. 112123.
[5] V. G. Brovkin and P. V. Vedenin, "Study of the microwave streamer evolution using a new semi-analytical model," *J. Appl. Phys.*, vol. 128, no. 11, Sep. 2020, Art. no. 113301.
[6] A. I. Saifutdinov and E. V. Kustova, "Dynamics of plasma formation and gas heating in a focused-microwave discharge in nitrogen," *J. Appl. Phys.*, vol. 129, no. 2, Jan. 2021, Art. no. 023301.
[7] D. G. Fearn, "The origin of the plasma in an electromagnetic shock tube," *J. Plasma Phys.*, vol. 2, no. 1, pp. 93–101, Feb. 1968.
[8] K. Xie, S. Guo, B. Sun, L. Quan, and Y. Liu, "Modeling and experimental study of low-frequency electromagnetic wave propagation in cylindrical enveloping plasma produced by a shock tube," *Phys. Plasmas*, vol. 26, no. 7, Jul. 2019, Art. no. 073509.
[9] J. Tian, P. Tang, P. Ma, L. Li, R. Li, Z. He, and B. Chen, "Single-frequency reflection characterisation of shock tube excited plasma," *AIP Adv.*, vol. 7, no. 8, Aug. 2017, Art. no. 085115.
[10] X. P. Lu and M. Laroussi, "Electron density and temperature measurement of an atmospheric pressure plasma by millimeter wave interferometer," *Appl. Phys. Lett.*, vol. 92, no. 5, Feb. 2008, Art. no. 051501.
[11] A. Boschi, N. Merzagora, and A. Tamburrano, "Microwave interferometry in high-temperature partially ionized dense gases," *J. Appl. Phys.*, vol. 43, no. 5, pp. 2160–2169, May 1972.
[12] S. Takeda and A. Funahashi, "Microwave reflection measurement of high electron densities of plasmas produced by shock waves," *Appl. Phys. Lett.*, vol. 8, no. 5, pp. 105–107, Mar. 1966.
[13] A. Cataldo and E. De Benedetto, "Broadband reflectometry for diagnostics and monitoring applications," *IEEE Sensors J.*, vol. 11, no. 2, pp. 451–459, Feb. 2011.
[14] J. Sánchez, B. Brañas, T. Estrada, E. de la Luna, and V. Zhuravlev, "Amplitude modulation reflectometry for large fusion devices," *Rev. Sci. Instrum.*, vol. 63, no. 10, pp. 4654–4656, Oct. 1992.
[15] E. de la Luna, J. Sanchez, V. Zhuravlev, I. G. Cortés, G. R. Hanson, J. B. Wilgen, J. H. Harris, J. Dunlap, R. Kaita, B. Leblanc, G. R. Tynan, L. Schmitz, and L. Blush, "First results with amplitude modulation reflectometry on the PBX-M tokamak," *Rev. Sci. Instrum.*, vol. 66, no. 1, pp. 403–405, Jan. 1995.
[16] P. Buratti, M. Zerbini, Y. Brodsky, N. Kovalev, and A. Shtanuk, "Amplitude modulation reflectometry system for the FTU tokamak," *Rev. Sci. Instrum.*, vol. 66, no. 1, pp. 409–411, Jan. 1995.
[17] T. Estrada, J. Sánchez, B. V. Milligen, L. Cupido, A. Silva, M. E. Manso, and V. Zhuravlev, "Density profile measurements by AM reflectometry in TJ-II," *Plasma Phys. Controlled Fusion*, vol. 43, no. 11, pp. 1535–1545, Oct. 2001.
[18] S.-H. Seo, J. Park, H. M. Wi, W. R. Lee, H. S. Kim, T. G. Lee, Y. S. Kim, J.-S. Kang, M. G. Bog, Y. Yokota, and A. Mase, "Development of frequency modulation reflectometer for Korea superconducting tokamak advanced research tokamak," *Rev. Sci. Instrum.*, vol. 84, no. 8, Aug. 2013, Art. no. 084702.
[19] O. Bogar, J. Zajac, F. Zacek, M. Varavin, M. Hron, R. Panek, and A. Silva, "Microwave reflectometer for density profile and turbulence measurements on the COMPASS tokamak," *Rev. Sci. Instrum.*, vol. 91, no. 1, Jan. 2020, Art. no. 013515.
[20] C. A. J. Hugenholtz and S. H. Heijnen, "Pulse radar technique for reflectometry on thermonuclear plasmas," *Rev. Sci. Instrum.*, vol. 62, no. 4, pp. 1100–1101, Apr. 1991.

[21] B. I. Cohen, E. B. Hooper, T. B. Kaiser, E. A. Williams, and C. W. Domier, "Modeling of ultra-short-pulse reflectometry," *Phys. Plasmas*, vol. 6, no. 5, pp. 1732–1741, May 1999.
[22] B. Li, H. Li, Z. Chen, C. Luo, H. Wang, S. Geng, L. Feng, Q. Liu, and W. Liu, "Pulse compression radar reflectometry to measure electron density in plasma with parasitic reflections," *Rev. Sci. Instrum.*, vol. 79, no. 7, Jul. 2008, Art. no. 073504.
[23] V. L. Ginzburg, *The Propagation of Electromagnetic Waves in Plasmas*. New York, NY, USA: Pergamon, 1970.
[24] C. H. Papas, *Theory of Electromagnetic Wave Propagation*. New York, NY, USA: Dove, 2005.
[25] J. Yao, Z. Yu, C. Yuan, Z. Zhou, X. Wang, and A. A. Kudryavtsev, "The influence of plasma distribution on microwave reflection in a plasma-metal model," *IEEE Trans. Plasma Sci.*, vol. 48, no. 2, pp. 359–363, Feb. 2020.
[26] C. X. Yuan, Z. X. Zhou, and H. G. Sun, "Reflection properties of electromagnetic wave in a bounded plasma slab," *IEEE Trans. Plasma Sci.*, vol. 38, no. 12, pp. 3348–3355, Dec. 2010.
[27] B. Bai, X. Li, J. Xu, and Y. Liu, "Reflections of electromagnetic waves obliquely incident on a multilayer stealth structure with plasma and radar absorbing material," *IEEE Trans. Plasma Sci.*, vol. 43, no. 8, pp. 2588–2597, Aug. 2015.
[28] A. Rokhlenko, "The reflection of electromagnetic waves by a conducting surface shielded with a plasma layer," *IEEE Trans. Plasma Sci.*, vol. 24, no. 1, pp. 182–186, Feb. 1996.
[29] L. Li, H. Hu, P. Tang, R. Li, B. Chen, and Z. He, "Compact dielectric constant characterization of low-loss thin dielectric slabs with microwave reflection measurement," *IEEE Antennas Wireless Propag. Lett.*, vol. 17, no. 4, pp. 575–578, Apr. 2018.
[30] L. Li, H. Hu, P. Tang, B. Chen, and Z. He, "A microwave reflection method to determine the complex permittivity of time-varying plasma," in *Proc. IEEE Int. Symp. Antennas Propag., USNC/URSI Nat. Radio Sci. Meeting*, Boston, MA, USA, Jul. 2018, pp. 1071–1072.

LUTONG LI (Student Member, IEEE) received the B.S. degree in electronic engineering from the University of Electronic Science and Technology of China (UESTC), Chengdu, China, in 2014, where he is currently pursuing the Ph.D. degree in electronic science and engineering. His current research interests include electromagnetic and microwave theory, antennas, microwave and millimeter measurements, plasma diagnostics, and so on.

HAOQUAN HU received the B.S. and M.S. degrees in electronic engineering from the University of Electronic Science and Technology of China (UESTC). He is currently a Professor with UESTC. His research interests include antenna design, electromagnetic compatibility and protection, and so on.

PU TANG received the M.S. degree from the University of Electronic Science and Technology of China (UESTC). He is currently a Professor with UESTC. His research interests include microwave and millimeter wave measurements, plasma characterization, antenna design, and electromagnetic compatibility.

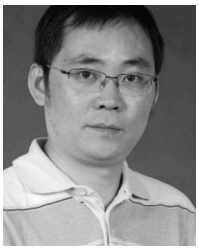

BO CHEN received the B.S. degree from the University of Electronic Science and Technology of China (UESTC). He is currently an Associate Professor with UESTC. His research interests include microwave and millimeter wave measurement, antenna design, electromagnetic compatibility and protection, and so on.

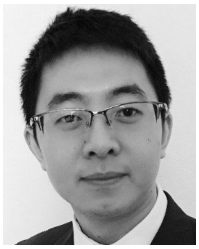

JING TIAN (Member, IEEE) received the M.S. degree in electrical engineering from the Tampere University of Technology, Finland, and the Ph.D. degree in electronic engineering from the Queen Mary University of London, U.K. He is currently a Lecturer with the University of Electronic Science and Technology of China (UESTC). His research interests include electromagnetic metamaterials, graphene, liquid crystal, and so on based EM devices.

BIXIAO JIANG received the B.S. and M.S. degrees in electromagnetic field and wireless technique from the University of Electronic Science and Technology of China, Chengdu, Sichuan, China, in 2016 and 2019, respectively, where he is currently pursuing the Ph.D. degree in electronic and communication engineering. His research interests include electromagnetic metasurfaces design and electromagnetic scattering of plasma.